


RESEARCH

Open Access



AIM2 promotes irradiation resistance, migration ability and PD-L1 expression through STAT1/NF- κ B activation in oral squamous cell carcinoma

Hui-Wen Chiu^{1,2,3†} , Hsin-Lun Lee^{4,5}, Hsun-Hua Lee^{6,7,8}, Hsiao-Wei Lu^{1,9,10}, Kent Yu-Hsien Lin^{11,12,13}, Yuan-Feng Lin^{1,14†} and Che-Hsuan Lin^{10,15*}

Abstract

Background Radioresistance and lymph node metastasis are common phenotypes of refractory oral squamous cell carcinoma (OSCC). As a result, understanding the mechanism for radioresistance and metastatic progression is urgently needed for the precise management of refractory OSCC. Recently, immunotherapies, e.g. immune checkpoint inhibitors (ICIs), were employed to treat refractory OSCC; however, the lack of predictive biomarkers still limited their therapeutic effectiveness.

Methods The Cancer Genome Atlas (TCGA)/Gene Expression Omnibus (GEO) databases and RT-PCR analysis were used to determine absent in melanoma 2 (AIM2) expression in OSCC samples. Colony-forming assay and trans-well cultivation was established for estimating AIM2 function in modulating the irradiation resistance and migration ability of OSCC cells, respectively. RT-PCR, Western blot and flow-cytometric analyses were performed to examine AIM2 effects on the expression of programmed death-ligand 1 (PD-L1) expression. Luciferase-based reporter assay and site-directed mutagenesis were employed to determine the transcriptional regulatory activity of Signal Transducer and Activator of Transcription 1 (STAT1) and NF- κ B towards the AIM2-triggered PD-L1 expression.

Results Here, we found that AIM2 is extensively upregulated in primary tumors compared to the normal adjacent tissues and acts as a poor prognostic marker in OSCC. AIM2 knockdown mitigated, but overexpression promoted, radioresistance, migration and PD-L1 expression via modulating the activity of STAT1/NF- κ B in OSCC cell variants. AIM2 upregulation significantly predicted a favorable response in patients receiving ICI treatments.

Conclusions Our data unveil AIM2 as a critical factor for promoting radioresistance, metastasis and PD-L1 expression and as a potential biomarker for predicting ICI effectiveness on the refractory OSCC.

Keywords Radioresistance, Metastasis, PD-L1, AIM2, Immune checkpoint inhibitors, Oral squamous cell carcinoma

[†]Hui-Wen Chiu and Yuan-Feng Lin are equally contributed to this study.

*Correspondence:

Che-Hsuan Lin

d119105002@tmu.edu.tw

Full list of author information is available at the end of the article



© The Author(s) 2024. **Open Access** This article is licensed under a Creative Commons Attribution 4.0 International License, which permits use, sharing, adaptation, distribution and reproduction in any medium or format, as long as you give appropriate credit to the original author(s) and the source, provide a link to the Creative Commons licence, and indicate if changes were made. The images or other third party material in this article are included in the article's Creative Commons licence, unless indicated otherwise in a credit line to the material. If material is not included in the article's Creative Commons licence and your intended use is not permitted by statutory regulation or exceeds the permitted use, you will need to obtain permission directly from the copyright holder. To view a copy of this licence, visit <http://creativecommons.org/licenses/by/4.0/>. The Creative Commons Public Domain Dedication waiver (<http://creativecommons.org/publicdomain/zero/1.0/>) applies to the data made available in this article, unless otherwise stated in a credit line to the data.

Introduction

Oral squamous cell carcinoma (OSCC) belongs to head and neck squamous cell carcinoma and accounts for 92–95% of oral malignancies [1]. The risk factors for OSCC are smoking, alcohol, betel nut chewing, nutritional deficiencies, and human papillomavirus (HPV) infection. Surgery alone or in combination with adjuvant radiotherapy with or without chemotherapy is the primary regimen for OSCC currently [2]. Recently, immunotherapy was developed to combat OSCC with no curative surgical and radiotherapeutic/chemotherapeutic treatment options [3]. Nevertheless, radioresistance/chemoresistance and the lack of biomarkers to predict the therapeutic effectiveness of immunotherapy impacted the clinical management of OSCC. As a result, understanding the molecular mechanism for radioresistance/chemoresistance and identifying valuable biomarkers for predicting the efficacy of immunotherapy are urgently needed.

Absent in melanoma 2 (AIM2) is one of the inflammatory members and acts as an innate immune sensor for double-strand DNA released from the invading pathogens. The assembly of AIM2 inflammasome promotes the secretion of interleukin-1 β (IL-1 β) and IL-18 and the induction of cell death through pyroptosis [4, 5]. The oncogenic role of AIM2 remains controversial in different cancer types. AIM2 upregulation has been correlated with a good prognosis [6] and suppresses epithelial–mesenchymal transition (EMT) via modulating PI3K/Akt and inflammasome pathways in colorectal cancer [7, 8]. Similarly, AIM2 could mitigate tumor growth and metastatic progression by inhibiting the PI3K/Akt/mTOR pathway in gastric cancer [9] and osteosarcoma [10]. The loss of AIM2 also promoted hepatocarcinoma progression through activation of the mTOR-S6K1 pathway [11] and EMT process [12]. In contrast, AIM2 upregulation promoted cell growth, metastasis and immunosuppression through the inflammasome-dependent pathway and correlated with poor survival in non-small cell lung cancer [13, 14], melanoma [15] and triple-negative breast cancer [16]. Besides, AIM2 was found to trigger renal cell carcinoma progression and sunitinib resistance through FOXO3a-ACSL4 axis-regulated ferroptosis [17]. In OSCC, the increased levels of AIM2 have been correlated with tumor growth and lymph node metastasis [18, 19]; however, the molecular mechanism remains largely unknown.

Consequently, this study aimed to investigate the involvement of AIM2 in the molecular mechanism for irradiation resistance, metastatic progression and immunomodulation in OSCC. Here, we find that AIM2 upregulation is commonly detected in primary tumors compared to normal adjacent tissues and refers to a poor

response to radiotherapy in OSCC patients. Moreover, the artificial alteration of AIM2 expression causally affected the irradiation resistance, migration ability and programmed death-ligand 1 (PD-L1) expression in OSCC cells. Computational simulation by the Gene Set Enrichment Analysis program and cell-based assays revealed that AIM2 upregulation reinforces the transcriptional regulatory activity of STAT1/NF- κ B towards the PD-L1 gene and fosters the metastatic and radioresistant phenotypes in OSCC cells. Fortunately, the increased levels of AIM2 highly correlate with a favorable responsiveness to immune checkpoint inhibitors, which provides an opportunity to combat those refractory OSCC with AIM2 upregulation in future clinics.

Materials and methods

Collection of clinical data and samples

The clinical information and transcriptional profiling data of head and neck squamous cell carcinoma (HNSCC) patients derived from The Cancer Genome Atlas (TCGA) and OSCC patients derived from the GSE42743 dataset were obtained from UCSC Xena website (UCSC Xena. Available online: <http://xena.ucsc.edu/welcome-to-ucsc-xena/>) and the Gene Expression Omnibus (GEO) database on the NCBI website, respectively. Primary tumors and normal adjacent tissues of OSCC patients were provided by Taipei Medical University Biobank and collected with institutional review board approval (N202204007) and the Declaration of Helsinki.

Cell culture

Oral cancer cell lines HSC2, HSC3, HSC4 and SAS were obtained from the Japanese Collection of Research Bioresources (JCRB) Cell Bank cultivated in Eagle's minimal essential medium supplemented with 10% fetal calf serum and 1% (w/v) Penicillin–Streptomycin at 37 °C with 5% CO₂. All culture reagents were purchased from Gibco (Grand Island, NY, USA).

Irradiation exposure

Cells (70% confluence) cultivated in 25-T flasks were exposed to 6 MV X-rays using a linear accelerator (Digital M Mevatron Accelerator, Siemens Medical Systems, CA, USA) at a 4 Gy/min dose rate. To ensure electronic equilibrium and full backscatter, a tissue-equivalent bolus (2 cm) was placed on top of and tissue-equivalent material (10 cm) was placed under the 25-T flasks, respectively.

Colony formation assay

Cells (2×10^3) without or with irradiation exposure at 4 Gy were seeded on the 6-well plates and cultured for two weeks. At the end of cultivation, the cells were fixed

with 80% ethanol prior to crystal violet (0.1%) staining for 10 min. After several wash steps, the remaining crystal violet was solubilized by using 30% acetic acid and its optical density was measured at 595 nm wavelength by a photometer.

Cell migration assay

Trans-well cultivation was performed by Boyden Chamber Assay (NeuroProbe, Gaithersburg, MD, USA) according to the procedure as shown in our previous report [14]. For neutralization of IL-1 β , AIM2-overexpressing SAS cells (1.5×10^4) were pre-treated without or with rabbit anti-IL-1 β (#41,059, SAB, Greenbelt, MD, USA) and non-immunized control (#10,119-T52/#CR1, Sino Biological, Beijing, China) polyclonal antibodies at 10 μ g/ml for 24 h before the trans-well culture for 16 h. Giemsa solution was used to stain the migrated cells after the removal of non-migrated cells. The stained cells were observed under an optical microscope and quantified in four random areas at 400 \times magnification.

Plasmid construction, lentiviral particle preparation and lentivirus infection

Human AIM2 cDNA clone (HG11654-UT) was purchased from Sino Biological Inc. (Beijing, China) and amplified by using the sticky-end polymerase chain reaction (PCR) method with two paired primers (primer #1: CTAGCATGGAGAGTAAATACAAGGAGATACTCTTG and CCTAIGT TTTTTTTTGGCCTTAATAACC, primer #2: CATGGAGAGTAAATACAAGGAGATACTCTTG and AATTCCTATGTTTTTTTTTTGGCCTTAATAACC) to generate the PCR products displaying cohesive ends compatible with NheI/EcoRI restriction sites. The sticky-end PCR products were the subclone into the lentiviral shuttle vector pLAS3w/puro using NheI/EcoRI restriction sites. The production of lentiviral particles containing without or with the AIM2 gene was performed through collaboration with the National RNAi Core Facility at Academia Sinica in Taiwan. The pLKO.1/puro plasmid containing non-silencing control (oligo sequence: CCGGACACTCGAGCACTTTTTG) and AIM2 shRNA clones (target sequence: sh1_CCCGCTGAACATTATCAGAAA; sh2_CCAACTGGTCTAA GCAGCATT) packaged in lentiviral particles were also obtained from the National RNAi Core Facility. Cells with 50% confluence cultivated in the 6-well plates were incubated with the conditioned medium containing polybrene (Santa Cruz) at 5 μ g/ml and then infected with the lentiviral particles containing without (non-silencing or vector control) or with AIM2 shRNAs or exogenous AIM2 gene at a multiplicity of infection (MOI) of 3–10. Puromycin (10 μ g/ml) selection was finally performed to generate stable clones. Western blot analysis and reverse

transcription-polymerase chain reaction (RT-PCR) were used to confirm AIM2 knockdown and overexpression efficiency in the puromycin-resistant cells.

RT-PCR

Total RNA was extracted by TRIzol extraction kit (Invitrogen) from the tested cells. M-MLV reverse transcriptase (Invitrogen) was employed for converting total RNA (5 μ g) to cDNA which was then amplified by PCR method using Taq-polymerase (Protech) with paired primers (for AIM2, forward-CTGCACAAAAGTCTCTCCTCATG and reverse-GGCTGAGTTTGAAGCGTGTTGAT C; for PD-L1, forward-GCTGCACTTCAGATCACAGATGTG and reverse-GTGTTGATTCTCAGT GTGCTGGTC; for GAPDH, forward-AGGTCGGAGTCAACGGATTG and reverse-GTGATGGC ATG GACTGTGGTC).

Western blot and dot blot assays

For Western blot analysis, aliquots of cell lysate (20–100 μ g) were subjected to SDS gel electrophoresis and then transferred to PVDF membranes. For dot blot analysis, culture media (200 μ L) were loaded into the well of dot blot apparatus and then transferred to nitrocellulose membrane by suction. The membranes were then immersed in the blocking buffer [5% bovine serum albumin for Western blot analysis against the phosphorylated protein and dot blot analysis or 5% skim milk in Tris buffer saline containing 0.1% Tween-20 (TBST)] for 2 h at room temperature or overnight at 4 $^{\circ}$ C with a gentle agitation. After blocking step, the membranes were further incubated with primary antibodies against PD-L1 (GTX635975, GeneTex, Hsinchu, Taiwan), phosphorylated (Ser536) NF- κ B (#3033)/NF- κ B (#6956)/phosphorylated (Tyr701) STAT1 (#9167)/STAT1 (#9172) (Cell Signaling, Danvers, MA, USA) and GAPDH (#PA0212, AbFrontier, Seoul, Korea), IL-1 β (#41,059, SAB) overnight at 4 $^{\circ}$ C. After the incubation, the membranes were washed several times with TBST followed by another incubation with a horseradish peroxidase-labeled secondary antibody for 1 h at room temperature. Immunoblots were then visualized by an enhanced chemiluminescence system (Amersham Biosciences, Tokyo, Japan).

Flow-cytometric analysis

Cells (1×10^7) from the designed experiments were collected by using dislodging solution (0.15 g disodium EDTA, 4.0 g NaCl, 0.28 g sodium bicarbonate, 0.5 g dextrose and 0.2 g KCl dissolved in 500 ml double distilled water and filter-sterilized) and stained with Brilliant Violet 605TM anti-human CD274 (PD-L1, #329,706, Biolegend, San Diego, CA, USA) antibody and its isotype IgG control antibody (2 μ l of each) for 20 min. After several

washes with phosphate-buffered saline, the stained cells were subjected to Flow-cytometric analysis.

Enzyme-linked immunosorbent assay (ELISA)

The secreted IL-1 β protein levels in the OSCC cell variant were detected by the commercial ELISA kits (Quantikine[®] ELISA, R&D Systems, Minneapolis, MN, USA) according to the manufacturer's protocol.

Luciferase reporter assay and site-directed mutagenesis

Firefly luciferase reporter vectors harboring an interferon-gamma (IFN γ) activation site (GAS), pGL4[Luc2P/GAS-RE/Hygro] and NF- κ B-binding element, pGL4.32[luc2P/NF- κ B-RE/Hygro] were purchased from Promega (Madison, WI, USA), and containing PD-L1 promoter region (– 1 to 1000 bp) was obtained from Addgene (Watertown, MA, USA). Site-directed mutagenesis for GAS and NF- κ B-binding element within PD-L1 promoter was performed by PCR with the paired primers (for GAS, 1st run_forward-CCATATGGCTTTGGTTTTATTCTAAGGAGTAGGTGTGTGTGTGTGTGTATGG and reverse-CCATACACACACACACACACCTACTCCTTAGAATAAAAACCAAA GCCATATGG, 2nd run_forward-GACCCATATGGCTTTGGTTTTACCTTAAGGAGTAGGTGT GTGTGTGTG and reverse-CACACACACACCTACTCCTTAA GGTA AAAACCAAGCCAT ATGGGTC; for NF- κ B-binding element, 1st run_forward-CTTCATTTGCTT TGTCATTA AAAAGAA CTGAAAATCCCGAGCTAC ATCTTTTAAGAATGCTCAG and reverse-CTGAGC ATTCTTAAA AGATGTAGCTCGGGATTTTCAGTTCTTTAATGACAAAGCAAATGAAG, 2nd run_forward-ATAATGAAACTTCATTTGCTTTGTCATTA AAATTCTGAAAATCCCGAGCTACATCTTTTAAG AATG and reverse-CATTCCTAAAAGATGTAGCTC GGGATTTTCAGAAATTTTAATGACAA AGCAAA TGAAGTTTCATTAT) using a *pfu* DNA polymerase kit (Stratagene, La Jolla, CA, USA). The methylated parental DNA template was removed by the treatment with *DpnI* endonuclease (New England BioLabs, Hitchin, Hertfordshire, UK). Luciferase reporter assay was performed by co-transfecting cells (70% confluence) with the designed firefly luciferase reporter vector at 0.25 μ g and control *Renilla* luciferase-expressing vector (p4.74-RLuc, Promega) at 0.0125 μ g using Lipofectamine 2000 (Invitrogen, Thermo Fisher Scientific, Waltham, MA, USA) according to the manufacturer's protocol. Post-transfection for 24 h, cells were lysed in Dual-Glo[™] Luciferase reagent. Luciferase activities were detected by Dual-Glo[®] Luciferase Assay (Promega) according to the manufacturer's protocol. The luminescent intensities of firefly luciferase derived from the tested cells were normalized to that of co-transfected *Renilla* luciferase.

Kaplan–Meier analysis

The Kaplan–Meier survival curves were generated from the K–M Plotter website according to the method reported by Lanczky A and Györffy B [20]. The best cutoff values, stratifying patients into the low and high-expression groups, were determined by the highest hazard ratio in the Cox regression test and the lowest false discovery rate (FDR) in the Benjamini–Hochberg test.

Gene Set Enrichment Analysis (GSEA)

GSEA software (version 4.0.3) was downloaded from Molecular Signature Database (MSigDB, <https://www.gsea-msigdb.org/gsea/index.jsp>). We then determined whether priori-defined Hallmark gene sets from MSigDB were enriched in the AIM2-related gene signature generated by pre-ranking the somatic genes which were included in the GSE42743 microarray experiment with Pearson coefficient values from the tests of their co-expression with AIM2 gene in primary tumors of GSE42743 OSCC patients who received radiotherapy and was recorded as dead in the follow-up. The AIM2-related gene signature was analyzed by the GSEA Pre-ranked module with recommended default settings (1000 permutations and a classic scoring scheme). The enrichment score (ES), normalized enrichment score (NES), nominal p-value and FDR q-value were calculated by the methods reported by Aravind Subramanian et al. [21] and obtained from the GSEA report. The p and q values lower than 0.05 were considered as significant.

Analysis of tumor-infiltrating immune cells

TIMER2.0, a web server (<http://timer.cistrome.org/>), reported by Taiwen Li et al. [22] was used to estimate the correlation among AIM2 mRNA levels, tumor purity and immune cell infiltration levels in TCGA HNSCC samples. The TIME2.0 reports shown as a scatter plot were downloaded from the website.

Statistical analysis

SPSS Statistics 19 software (IBM, Armonk, NY, USA) was used to analyze statistical significance. Student t-test was used to estimate the statistical difference of AIM2 expression in primary tumors and normal tissues. The correlation among AIM2 mRNA levels, immune cell infiltration levels and other somatic gene expression levels were analyzed by Pearson's and nonparametric Spearman's tests in the detected primary tumors. Nonparametric Mann–Whitney U and Friedman tests were employed to estimate the two independent samples and three or more related samples, respectively. The p values lower than

0.05 were considered to be statistically significant in all experiments.

Results

AIM2 upregulation is extensively detected in primary tumors compared to normal adjacent tissues and correlates with poor sensitivity to radiotherapy in OSCC

We dissected the transcriptional profile of AIM2 in the normal tissues and primary tumors derived from head and neck squamous cell carcinoma (HNSCC) patients in The Cancer Genome Atlas (TCGA) database. The data showed that AIM2 expression in primary tumors is extensively higher than in normal tissues (Fig. 1A). Similar views were found in the paired normal and tumor tissues derived from TCGA HNSCC patients (Fig. 1A). Using the GSE42743 dataset, we also found that AIM2 upregulation is predominant in primary tumors compared to normal tissues or adjacent normal tissues from OSCC patients (Fig. 1B). Accordingly, RT-PCR results demonstrated that AIM2 expression is significantly ($p < 0.01$) elevated in primary tumors compared to the normal adjacent tissues from OSCC patients in Taipei Medical University Biobank (Fig. 1C and D). Kaplan–Meier analyses using a maximal risk condition demonstrated that AIM2 upregulation significantly ($p = 0.019$) was associated with a poorer overall survival in GSE42743 OSCC, but not TCGA HNSCC, patients who received radiotherapy (Fig. 1E). Accordingly, AIM2 upregulation was significantly ($p = 0.013$) correlated with a shorter overall survival time in GSE42743 OSCC patients who received radiotherapy and were recorded dead in the follow-up (Fig. 1F). However, there were no statistical significances in the correlation between AIM2 expression and overall survival time in the TCGA HNSCC cohorts who received radiotherapy regardless of survival status and GSE42743 OSCC patients who received radiotherapy and were recorded as alive in the follow-up (Fig. 1F).

AIM2 upregulation promotes radioresistance and metastatic potentials in OSCC cells

We next determined the endogenous mRNA levels of AIM2 by RT-PCR experiment in a panel of OSCC cell lines SAS, HSC2, HSC3 and HSC4. The data showed that HSC3 and HSC4 cells exhibit a relatively higher mRNA level of AIM2 than SAS and HSC2 cells (Fig. 2A). The endogenous mRNA levels of AIM2 were found to negatively associate with the cytotoxicity of irradiation (Fig. 2B) but positively correlate with cellular migration ability (Fig. 2C) in the tested OSCC cell lines. The knockdown of the AIM2 gene in HSC4 cells (Fig. 2D) dramatically restored the cellular sensitivity to irradiation treatment (Fig. 2E) and predominantly mitigated

the cellular migration ability (Fig. 2F). Conversely, the enforced expression of the exogenous AIM2 gene in SAS cells (Fig. 2G) robustly promoted radioresistance (Fig. 2H) and markedly enhanced the cellular migration ability (Fig. 2I).

AIM2 upregulation activates STAT1 and NF- κ B-related signaling cascades to potentiate PD-L1 expression in OSCC cells

To understand the possible mechanism underlying the AIM2-associated radioresistance in OSCC, Gene Set Enrichment Analysis (GSEA) was conducted to detect whether a series of priori-defined biological processes deposited in Hallmark gene sets from the Molecular Signature database were enriched in the gene rank of AIM2-related gene signature from primary tumors of GSE42743 OSCC patients who received radiotherapy and was recorded as dead in the follow-up. The Pearson coefficient values derived from the correlation among the mRNA levels of AIM2 and somatic genes included in the microarray chip of the GSE42743 dataset were used to generate a ranked order of somatic genes, which was defined as the AIM2-related gene signature (Fig. 3A). GSEA results indicated that the AIM2-related gene signature is highly correlated with the upregulation of interferon-gamma (IFN γ) responsive gene set, as well as TNF α -NF- κ B signaling axis-regulated gene set (Fig. 3B and C). By using the TIMER2.0 program, we found that AIM2 mRNA levels positively correlate with the infiltration levels of IFN γ -producing CD8+ T cells and nature killer (NK) cells and TNF α -secreting M1 macrophages in TCGA HNSCC samples (Fig. 3D). Since programmed death-ligand 1 (PD-L1) is one of the IFN γ -inducing genes, we further examined the co-expression of AIM2 and PD-L1 in TCGA HNSCC and GSE42743 OSCC samples. The data showed that AIM2 expression was positively associated with PD-L1 expression in TCGA HNSCC and GSE42743 OSCC samples (Fig. 3E). This positive correlation was more predominant in the GSE42743 OSCC samples derived from patients who received radiotherapy and were recorded dead in the follow-up (Fig. 3E).

We further determined the endogenous PD-L1 levels in the radiosensitive/poorly migrated SAS cells and radioresistant/highly migrated HSC4 cells. The data obtained from RT-PCR/Western blot analyses (Fig. 4A) and flow-cytometric analysis (Fig. 4B) revealed that HSC4 cells, compared to SAS cells, harbor higher endogenous mRNA/protein levels and membranous protein levels of PD-L1. Whereas AIM2 knockdown in HSC4 cells markedly inhibited PD-L1 expression (Fig. 4C), AIM2 overexpression predominantly promoted PD-L1 levels in SAS cells (Fig. 4D). To delineate if AIM2 expression can affect

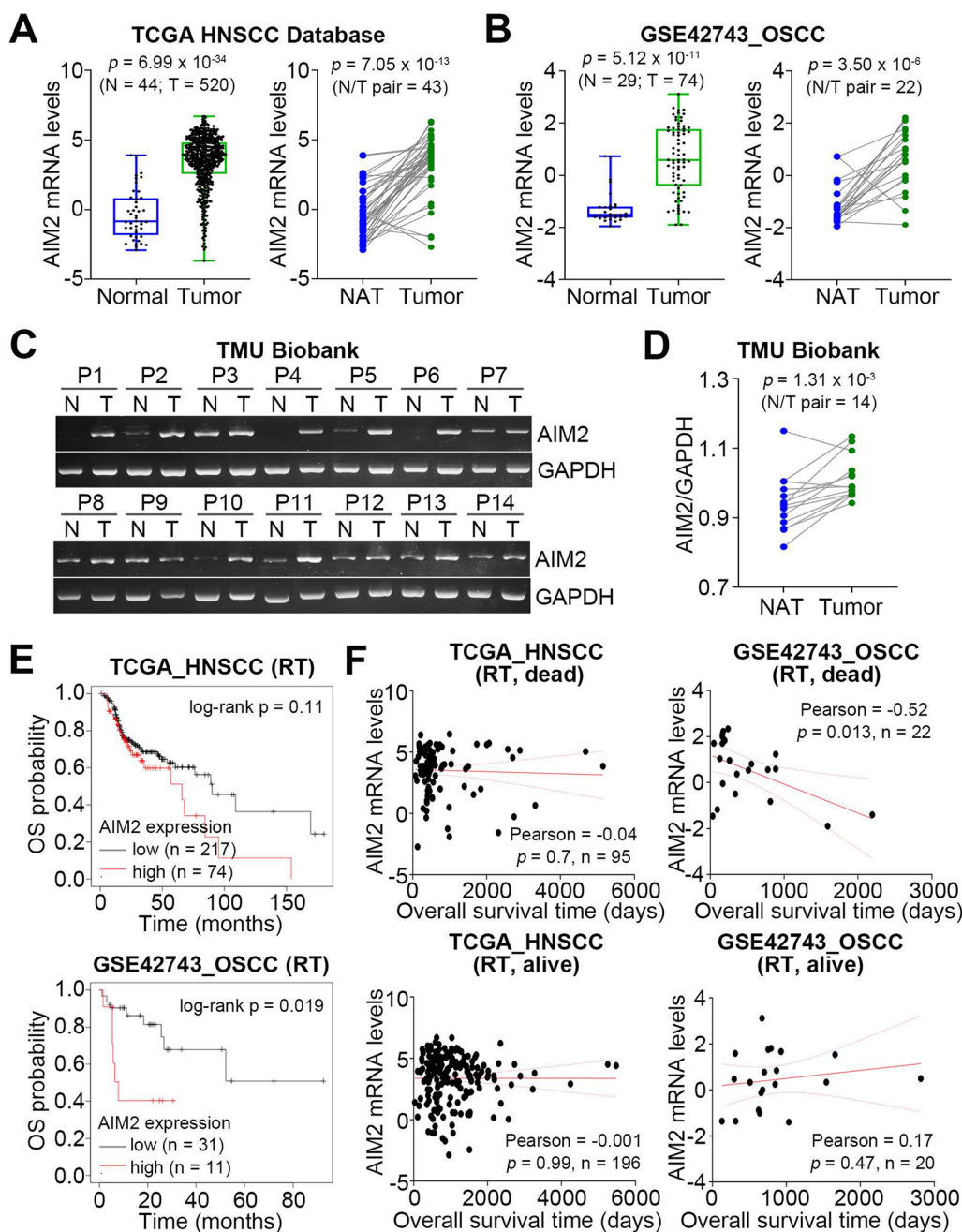


Fig. 1 AIM2 upregulation is highly detected in primary tumors compared to normal adjacent tissues and correlates with a poor response to radiotherapy in OSCC. **A** and **B** Boxplots and dot plots with line respectively present AIM2 mRNA levels in the unpaired normal tissues (N)/primary tumors (T) and paired normal adjacent tissues (NAT)/primary tumors derived from TCGA HNSCC (**A**) and GSE4273 OSCC (**B**) samples. **C** and **D** RT-PCR (**C**) and dot plots with lines (**D**) show the AIM2 gene expression in the paired primary tumors/normal adjacent tissues derived from OSCC samples in Taipei Medical University (TMU) Biobank. **E** Kaplan–Meier analyses for AIM2 mRNA levels using overall survival (OS) probability under a maximal risk condition against TCGA HNSCC (upper) and GSE42743 OSCC (lower) patients who received radiotherapy. **F** Scatter plots for the correlation between AIM2 mRNA levels in the respective primary tumors and overall survival time of TCGA HNSCC and GSE42743 OSCC patients receiving radiotherapy (RT) with the overall survival endpoint as alive or dead

the activity of IFN γ -STAT1 and TNF α -NF- κ B signaling pathways, we performed another Western blot analysis to examine the actively phosphorylated protein levels of

STAT1 and NF- κ B and luciferase reporter assays to determine the DNA-binding activity of STAT1 and NF- κ B. The data showed that AIM2 knockdown in HSC4 suppresses,

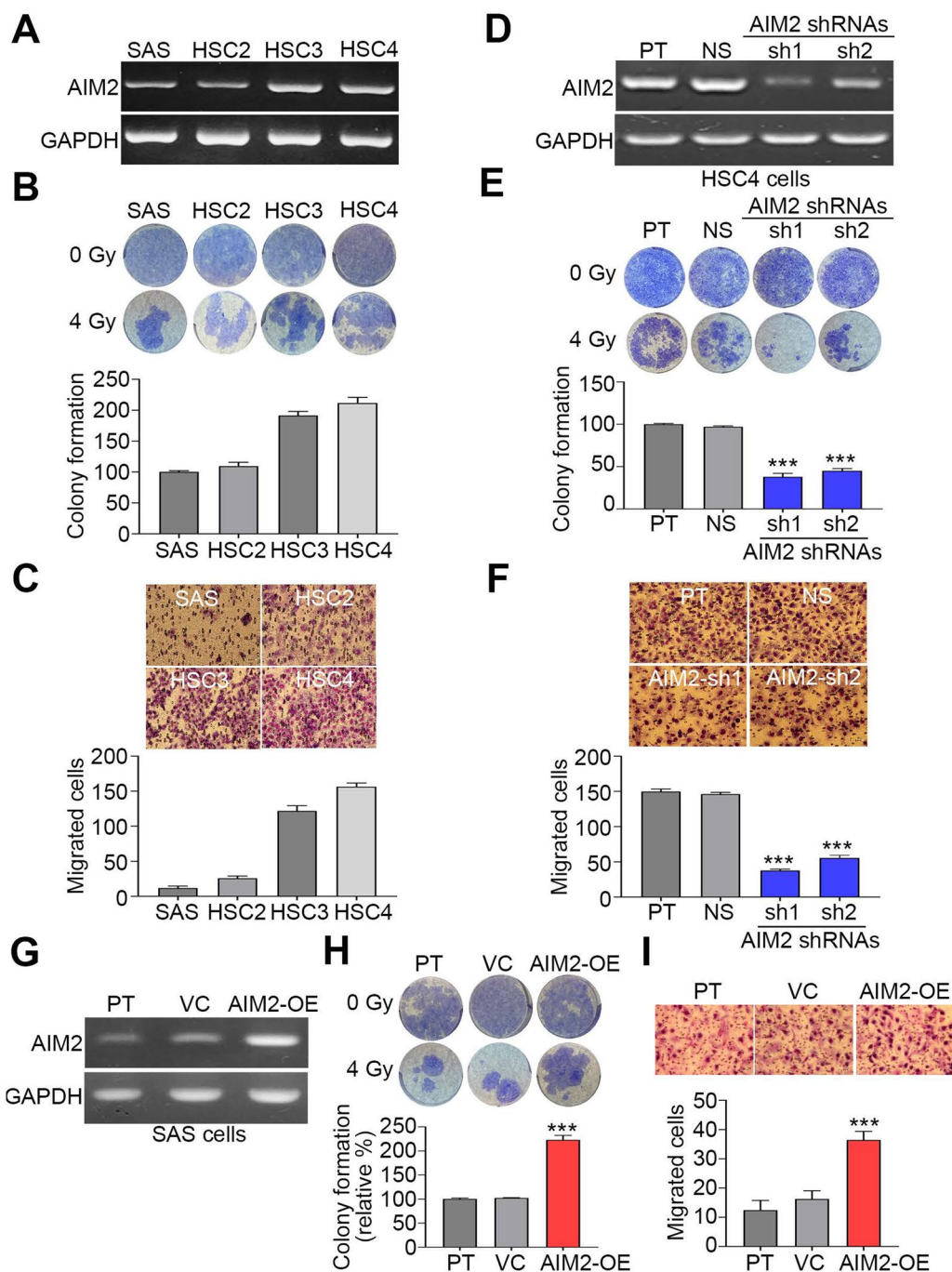


Fig. 2 AIM2 expression is associated with cellular irradiation resistance and migration ability in OSCC cells. **A–I** RT-PCR for the endogenous mRNA levels of AIM2 and GAPDH, crystal violet staining (upper)/histogram (lower) for colony formation post-treatment without or with irradiation at 4 Gy and Giemsa staining (upper)/histogram (lower) for the migrated cells in the tested OSCC cell lines (**A–C**), HSC4 cell variants (**D–F**) and SAS cell variants (**G–I**). In **A**, **D** and **G**, GAPDH was used as an internal control of the experiment. The abbreviations of PT, NS, VC and OE are parental, non-silencing, vector control and overexpression, respectively. *** $p < 0.001$

but AIM2 overexpression in SAS cells elevates the phosphorylated protein levels and the transcriptional regulator activity of STAT1 (Fig. 4E and F) and NF- κ B (Fig. 4G and H). To understand the transcriptional regulation of

STAT1 and NF- κ B towards the PD-L1 gene, we further established the luciferase-based promoter assay by sub-cloning PD-L1 promoter sequence (– 1 to – 1000 bp) into the upstream of the firefly luciferase gene (Fig. 4I).

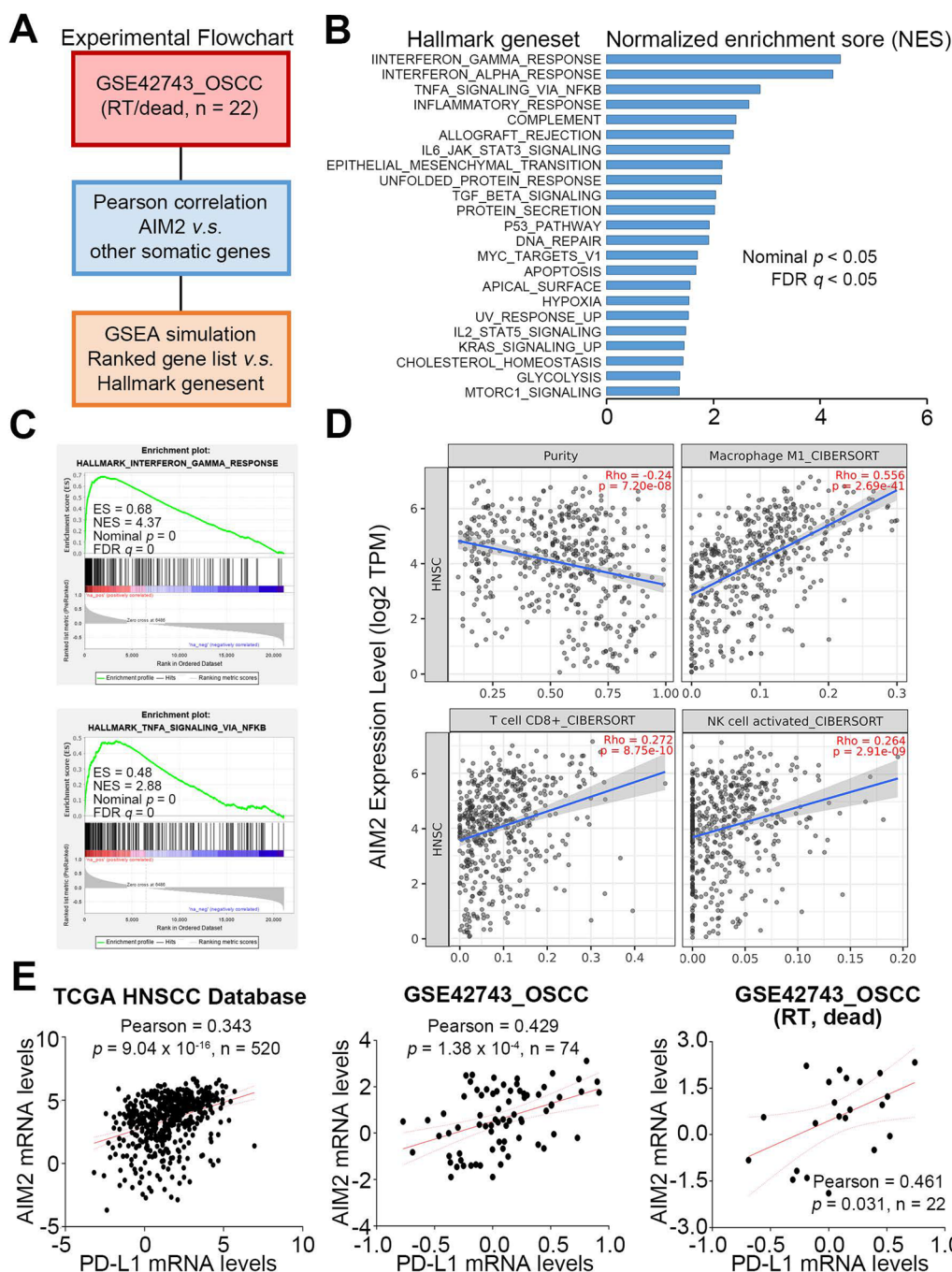


Fig. 3 AIM2 upregulation highly correlates with the activation of interferon and inflammation-related pathways and the expression of PD-L1 in the primary tumors derived from OSCC patients with a poorer responsiveness to radiotherapy. **A** Experimental flowchart for generating AIM2 gene signature and performing GSEA simulation. **B** Histogram for Hallmark genesets with positive NES and statistical significance (p and $q < 0.05$) in GSEA simulation against AIM2 gene signature. **C** The plot of enrichment score for IFN γ -responsive and TNF α /NF- κ B signaling axis-regulated genesets in GSEA simulation against AIM2 gene signature. **D** Scatter plot derived from TIMER2.0 for the correlation of AIM2 mRNA levels with tumor purity and infiltration levels of macrophages, CD8+T cells and NK cells against TCGA HNSCC. **E** Scatter plot for the co-expression of AIM2 and PD-L1 in TCGA HNSCC primary tumors (left) and GSE42743 OSCC samples derived from patients without (middle) or with (right) the indicated records. In **D** and **E**, the solid and dashed lines shown in red represent the 95% confidence bands (dashed) of the best-fit line (solid) in Simple Linear Regression

According to the previous report [23], we found a putative IFN γ -activated site (– 502 to – 510) which facilitates the binding of active STAT1 within the PD-L1 promoter sequence (Fig. 4I). Moreover, the in silico analysis by the PROMO program indicated a putative NF- κ B binding site (– 502 to – 510) in the targeted PD-L1 promoter sequence (Fig. 4I). Whereas AIM2 knockdown in HSC4 cells was dramatically suppressed, AIM2 overexpression in SAS cells predominantly enhanced the intracellular luciferase activities after the transfection with the plasmid containing a PD-L1 promoter-driven firefly luciferase gene (Fig. 4J). Furthermore, we performed the site-directed mutagenesis for IFN γ -activated site and NF- κ B binding site to verify the functional role of STAT1 and NF- κ B in regulating the transcription of the PD-L1 gene (Fig. 4I). Luciferase reporter assay by transfecting AIM2-overexpressing SAS cells with the firefly luciferase gene in conjunction with the different PD-L1 promoter variants demonstrated that the mutation of IFN γ activated site or/and NF- κ B binding site significantly ($p < 0.05$) reduced the intracellular luciferase activity (Fig. 4K). Similar views were also found in the AIM2-upregulated HSC3/HSC4 cells transfected with the firefly luciferase gene harboring the different PD-L1 promoter variants (Fig. 4H). These findings indicate that AIM2 upregulation fosters the transcription of PD-L1 by activating STAT1 and NF- κ B in the metastatic/radioresistant OSCC.

AIM2 upregulation promotes the secretion of IL-1 β , which activates STAT1/NF- κ B-related pathways to reinforce cellular irradiation resistance, migration ability and PD-L1 expression in OSCC cells

Interleukin-1 β (IL-1 β) secretion to the extracellular matrix is tightly regulated by inflammasome machinery. As a result, we next determined the extracellular protein levels of IL-1 β by dot blot analysis and a commercial ELISA kit. The data showed that AIM2 knockdown in HSC4 cells markedly reduces, but AIM2

overexpression in SAS cells predominantly elevates the secretion of IL-1 β (Fig. 5A). The inclusion of an IL-1 β -neutralizing antibody, not an isotype control antibody, significantly ($p < 0.05$) suppressed STAT1/NF- κ B activity, colony formation post-treatment with irradiation, cellular migration ability and PD-L1 expression in the AIM2-overexpressing SAS cells (Fig. 5B–E). Moreover, the pharmaceutical inhibition of NF- κ B by its specific inhibitor SN-50 dose-dependently mitigated colony formation post-treatment with irradiation, cellular migration ability and PD-L1 expression in the AIM2-overexpressing SAS cells (Fig. 5F–H).

AIM2 upregulation might be a valuable biomarker for predicting the anti-cancer effectiveness of immune checkpoint inhibitors on the metastatic/radioresistant OSCC

The data obtained from the ROC plotter demonstrated that AIM2 upregulation predicts a favorable response to immune checkpoint inhibitors (ICIs), particularly in patients receiving Pembrolizumab (anti-PD-1 antibody) and Ipilimumab (anti-CTLA4 antibody) (Fig. 6A). Although the expression of AIM2 in the primary tumors derived from non-responder and responder patients who received Nivolumab (anti-PD-1 antibody) and Atezolizumab (anti-PD-L1 antibody) treatment did not show a significant difference in ROC Plotter analysis (Fig. 6A), Kaplan–Meier plots under a maximal risk condition revealed that a higher level of AIM2 expression predominantly correlates with a good progression-free survival rate in cancer patients receiving these four ICIs (Fig. 6B).

Discussion

The inflammasome activation was thought to be involved in the tumor progression of radioresistant breast cancer [24]. The recent report indicated that SP1 transcriptionally activates NLRP6 inflammasome to trigger immune evasion and radioresistance in glioma cells [25]. AIM2 upregulation was found to predict a favorable prognosis

(See figure on next page.)

Fig. 4 AIM2 upregulation promotes PD-L1 expression via activating STAT1 and NF- κ B signaling pathways in OSCC cells. **A** and **B** RT-PCR (left)/Western blot analyses (right) for the endogenous mRNA/protein levels of PD-L1 and GAPDH (**A**) and histograms for the mean of fluorescent intensity (MFI) of isotype control (cyan) and PD-L1 (pink) antibodies in Flow-cytometric analysis (**B**) against SAS and HSC4 cells. **C** and **D** RT-PCR (upper)/Western blot analysis (middle) for the endogenous mRNA/protein levels of PD-L1 and GAPDH and histograms for the MFI of PD-L1 antibody normalized to control groups (NS and VC) in Flow-cytometric analysis against HSC4 (**C**) and SAS (**D**) cell variants. **E–H** Western blot analyses for phosphorylated STAT1/NF- κ B, total STAT1/NF- κ B and GAPDH protein levels (upper) and histograms for the DNA-binding activity of STAT1/NF- κ B normalized to control groups (NS and VC) in luciferase reporter assay (lower) against HSC4 (**E** and **G**) and SAS (**F** and **H**) cell variants. **I** Illustration for the locations and mutated nucleotides of NF- κ B binding site/IFN γ activated site in the PD-L1 promoter region subcloned into the upstream of the firefly luciferase gene. **J–H** Histograms for the normalized luciferase activity detected from HSC4/SAS cell variants (**J**), AIM2-overexpressing SAS cells (**K**) and HSC3/HSC4 cells (**H**) cells transfected with the PD-L1 promoter-driven firefly luciferase reporter vector without or with mutations at NF- κ B binding site and IFN γ activated site. In **A**, **C**, **D**, **E**, **F** and **G**, GAPDH was used as an internal control of experiments. The symbol “****” and different alphabets denote $p < 0.001$ and 0.05 , respectively

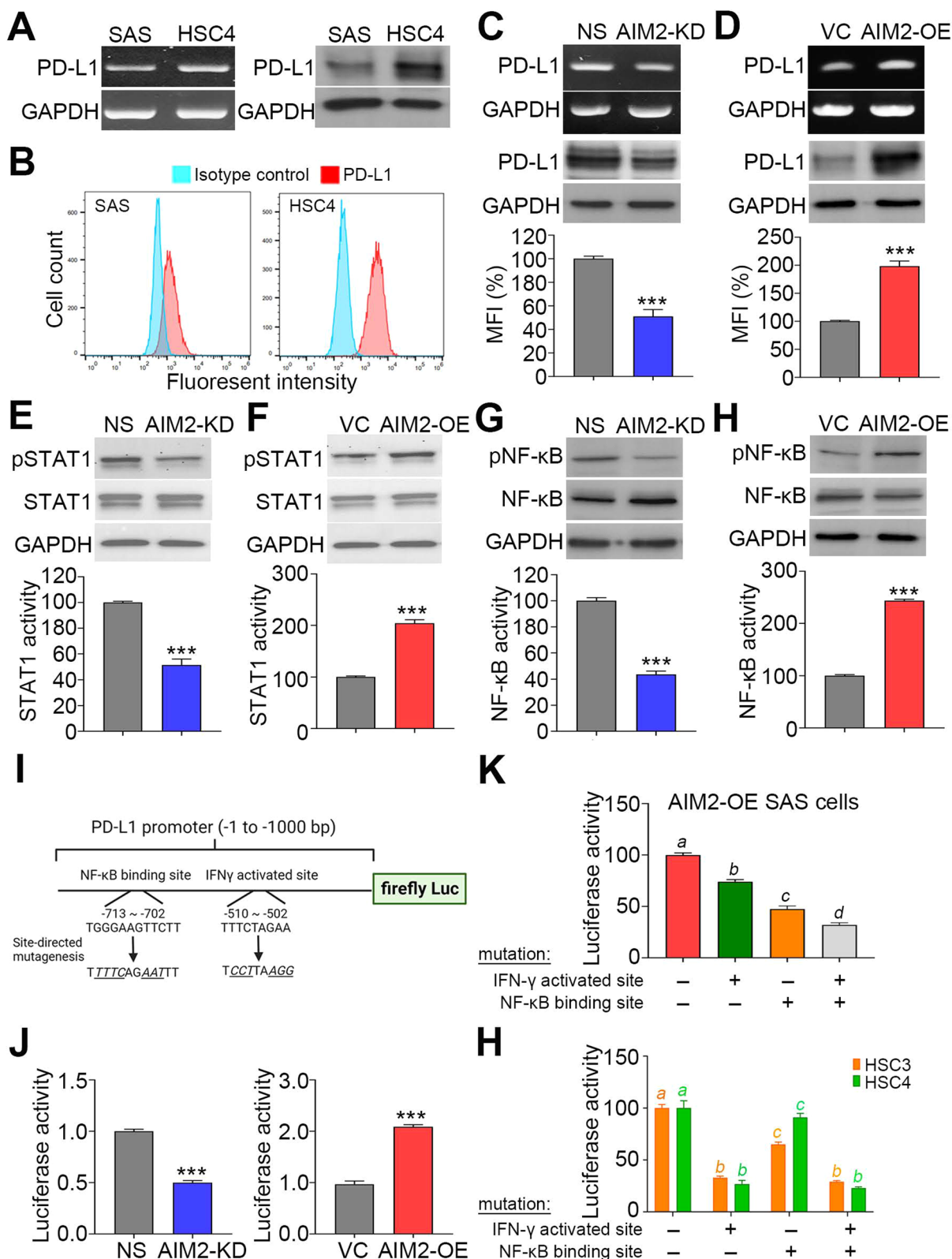


Fig. 4 (See legend on previous page.)

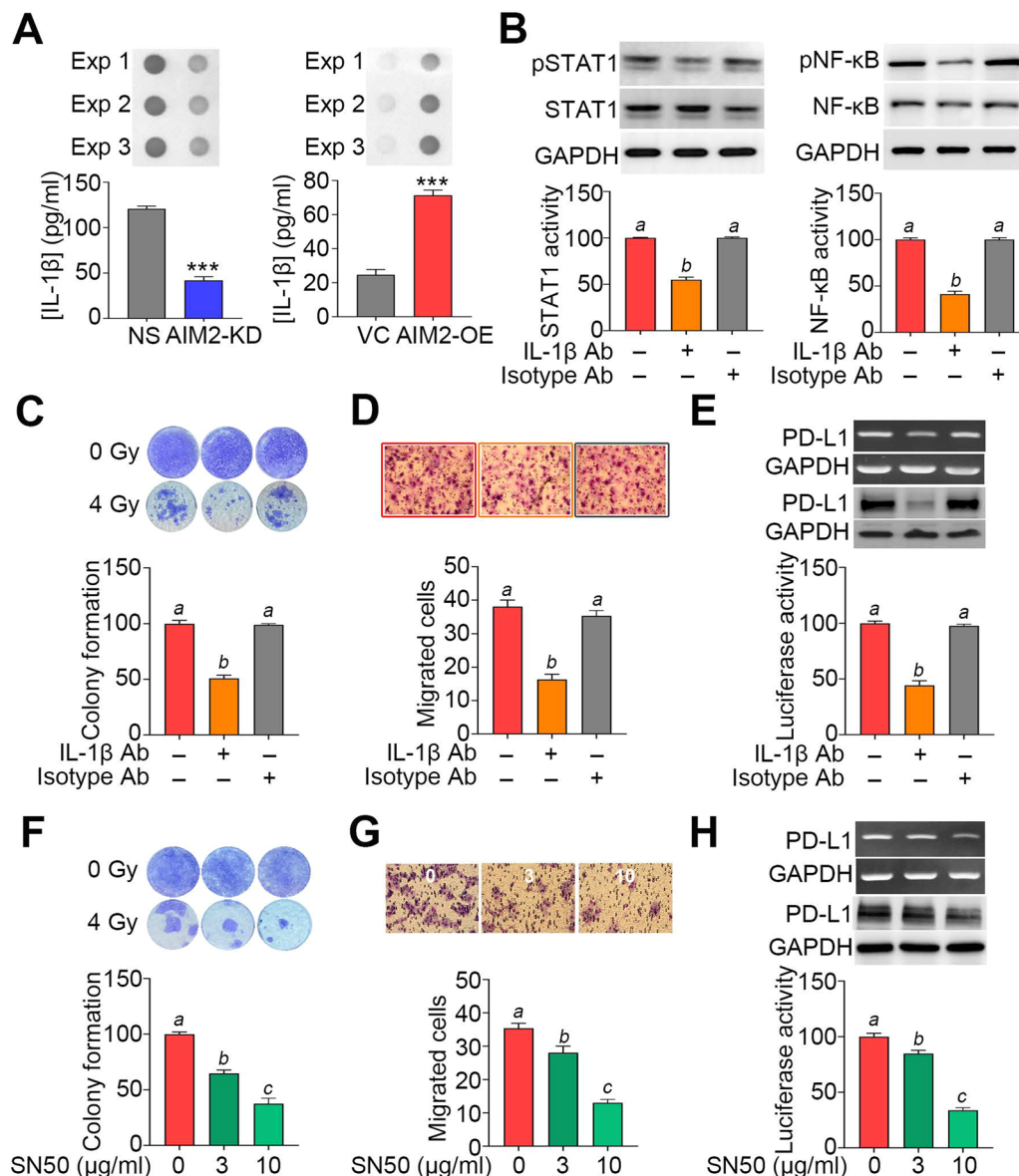


Fig. 5 The AIM2-triggered IL-1 β secretion positively regulates STAT1/NF- κ B activation, irradiation resistance, cellular migration ability and PD-L1 expression in OSCC cells. **A** Dot blot (upper) of three independent experiments (Exp) and histograms (lower) of ELISA results for the IL-1 β protein levels in the culture media from HSC4 (left) and SAS (right) cell variants. **B** Western blot analyses for phosphorylated STAT1/NF- κ B, total STAT1/NF- κ B and GAPDH protein levels (upper) and histograms for DNA-binding activity of STAT1/NF- κ B in luciferase reporter assays (lower) against the AIM2-overexpressing SAS cells treated without or with IL-1 β -neutralizing or isotype antibody (Ab, 10 μ g/ml of each). **C–H** Crystal violet staining (upper)/histogram (lower) for colony formation post-treatment without or with irradiation at 4 Gy, Giemsa staining (upper)/histogram (lower) for the migrated cells and RT-PCR/Western blot analyses for the mRNA/protein levels of PD-L1 and GAPDH (upper)/histograms for PD-L1 transcriptional activity in luciferase assays (lower) against the AIM2-overexpressing SAS cells cultivated in the absence or presence of IL-1 β -neutralizing/isotype antibody (**C–E**) and NF- κ B inhibitor SN50 at the indicated concentrations (**F–H**). In **B**, **E** and **H**, GAPDH was used as an internal control of experiments. The symbol “****” and different alphabets represent $p < 0.001$ and $p < 0.05$, respectively

in colorectal cancer [7, 8], gastric cancer [9] and osteosarcoma [10], but associated with cancer progression, e.g. tumor growth, metastasis and immunosuppression, in non-small cell lung cancer [13, 14], melanoma [15], triple-negative breast cancer [16] and renal cell carcinoma [17].

AIM2 upregulation due to promoter hypomethylation has been shown to play an oncogenic role [26] and the enforced expression of AIM2 promoted tumor growth and lymph node metastasis in OSCC [18, 19]. However, the molecular mechanism for the AIM2-promoted OSCC

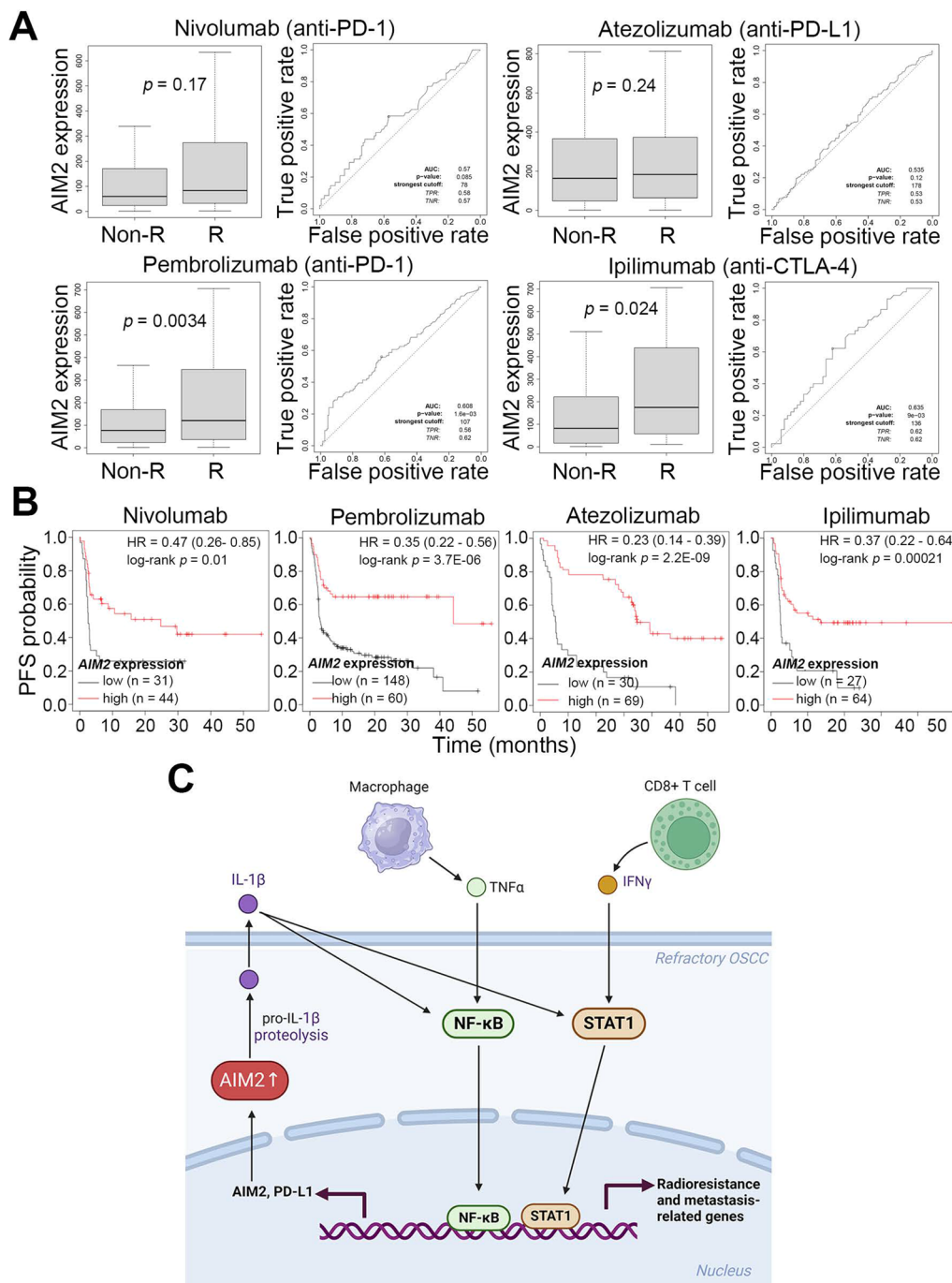


Fig. 6 AIM2 upregulation correlates with a favorable response in cancer patients receiving immune checkpoint inhibitors. **A** Box plots for AIM2 mRNA levels in the non-responder (non-R) and responder (R) and receiver operating characteristic (ROC) curve (right) for the predictive sensitivity of AIM2 expression in ROC Plotter cancer patients receiving the indicated ICIs. **B** Kaplan–Meier analyses for AIM2 mRNA levels using progression-free survival probability under a maximal risk condition against K-M Plotter cancer patients receiving the indicated ICIs. **C** A proposed model for the AIM2-promoted radioresistance, metastasis and PD-L1 expression in refractory OSCC

progression remains largely unknown. Here, we further show that AIM2 upregulation promotes radioresistance, metastasis and PD-L1 expression, probably through an

IL-1 β -triggered activation of STAT1 and NF- κ B pathways in refractory OSCC cells (Fig. 6C). The in silico analyses demonstrate that AIM2 upregulation fosters

the infiltration of IFN γ -producing CD8+ T cells and TNF α -secreting macrophages to reinforce the activation of IFN γ -STAT1 and TNF α -NF- κ B signaling pathways, which may ultimately force the expression of AIM2 and PD-L1, both are IFN γ -inducing genes [27, 28], in refractory OSCC cells (Fig. 6C). The formation of this signaling loop consequently potentiates the malignancy, e.g., radioresistance, metastasis and immune evasion, of OSCC. Fortunately, our findings provide a potential strategy to combat these refractory OSCC with AIM2 upregulation by immune checkpoint inhibitors Pembrolizumab and Ipilimumab.

NF- κ B activation was considered a critical trigger for radioresistance [29]. As a result, targeting NF- κ B activity was thought to be a potential strategy to combat cancer radioresistance [30]. Recent reports demonstrated that the activation of the TNF- α /NF- κ B signaling axis enhances the metastatic capacity and PD-L1 expression of OSCC [31, 32]. Inhibition of NF- κ B was found to mitigate the cellular invasive ability and restore the responsiveness to radiotherapy in glioblastoma [33]. In this study, GSEA simulation indicated that AIM2 upregulation highly correlates with the activation of TNF- α /NF- κ B pathway in OSCC tumors derived from patients recorded as dead in the follow-up after irradiation treatment. Besides, AIM2 overexpression promoted the pro-inflammatory cytokine IL-1 β which further reinforces the activation of the NF- κ B pathway in SAS cells. The blocking of the NF- κ B pathway restored the radiosensitivity and suppressed the cellular migration ability and PD-L1 expression in the AIM2-overexpressed SAS cells. Importantly, the activation of NF- κ B may also enhance the transcription of other pro-inflammatory factors, e.g., T cell/macrophage chemotaxis cytokine CXCL10 [34], and thereby promote the infiltration of those immune cells to the tumor microenvironment and reinforce the function of IFN γ -STAT1 and TNF α -NF- κ B signaling pathways in triggering the transcription of AIM2 and PD-L1 in refractory OSCC. Consequently, AIM2 upregulation likely reprograms the tumor immune microenvironment towards an immune-inflamed condition characterized by increased IFN γ signaling and PD-L1 expression [35] and is reported to be more responsive to ICI treatment [36].

The IFN γ -related gene signature was recently found to be capable of selecting melanoma patients who probably benefited from ICI treatment [37]. In this study, the *in silico* analyses revealed that AIM2 upregulation is extremely associated with the activation of IFN γ -responsive pathway in the radioresistant OSCC samples and the infiltration levels of IFN γ -producing immune cells in TCGA HNSCC samples. It has been shown that IFN γ can trigger the transcription of the PD-L1 gene via activating STAT1 [28]. Nevertheless, without IFN γ

supplement, the mutation of the STAT1-binding site within the PD-L1 promoter dramatically suppressed luciferase activity in the highly metastatic/radioresistant HSC3/HSC4 cells transfected with a plasmid containing PD-L1 promoter-driven firefly luciferase gene. In addition, the neutralization of IL-1 β moderately inhibited the activity of STAT1 in the AIM2-overexpressing SAS cells. Moreover, recent reports demonstrated that IL-1 β can activate the STAT1 pathway by negatively modulating ERK2 activation in the target cells [38] and synergistically elevates PD-L1 expression through the coordination with IFN γ in hepatocellular carcinoma [39]. Therefore, these findings implicate that AIM2 upregulation coordinates the activation of STAT1 and NF- κ B by triggering the secretion of IL-1 β through the AIM2 inflammasome machinery, thereby governing PD-L1 transcription in refractory OSCC.

TNF α plays a critical role in the onset of immune response and is produced mainly secreted by macrophages even though other immune and non-immune cells, e.g. fibroblast, can produce TNF α [40]. TNF α has been associated with the progression and prognosis of different cancer types by perturbing several signaling pathways, e.g., Erk1/2 and NF- κ B [32]. Besides, TNF α coordinated with IFN γ to promote MUC16 (CA125) expression in breast and ovarian cancer via the NF- κ B signaling axis [41]. Moreover, TNF α secreted from the infiltrating macrophages enhanced PD-L1 expression by activating NF- κ B, resulting in a poor prognosis in pancreatic cancer [42]. Here we found that AIM2 upregulation is highly associated with the activation of the TNF α -NF- κ B signaling axis, which is likely regulated by the infiltrated macrophages and constitutively elevates PD-L1 expression via IL-1 β -NF- κ B pathway in refractory OSCC. Therefore, these findings suggest that AIM2 expression could serve as a valuable biomarker for predicting the therapeutic effectiveness of TNF α and PD-L1-targeting agents and NF- κ B inhibitors in the refractory OSCC.

Although there were some ongoing clinical trials for ICIs in OSCC [43], the FDA approved nivolumab and pembrolizumab for patients with relapsed/metastatic HNSCC [44]. Here we find that AIM2 upregulation refers to a favorable progression-free survival rate in cancer patients receiving nivolumab, pembrolizumab, atezolizumab or ipilimumab monotherapy even though its upregulation was not significant for predicting the responsiveness of cancer patients who received nivolumab or atezolizumab monotherapy in ROC plot analysis. Therefore, our findings suggest that AIM2 might be a valuable biomarker for predicting the anti-cancer effectiveness of pembrolizumab and ipilimumab on the radioresistant/metastatic OSCC.

Conclusion

AIM2 upregulation may constitutively activate the IL-1 β -STAT1/NF- κ B signaling loop to elevate PD-L1 expression and probably trigger the infiltration of IFN γ and TNF α -producing immune cells to reinforce the activity of STAT1 and NF- κ B, respectively, in the refractory OSCC. Although further experiments are still needed to explore the role of AIM2 in promoting the reprogramming of tumor immune microenvironment, our results suggest that ICIs could be an effective therapeutic strategy to combat the refractory OSCC with AIM2 upregulation.

Abbreviations

OSCC	Oral squamous cell carcinoma
HNSCC	Head and neck squamous cell carcinoma
ICIs	Immune checkpoint inhibitors
AIM2	Absent in melanoma 2
PD-L1	Programmed death-ligand 1
STAT1	Signal Transducer and Activator of Transcription 1
HPV	Human papillomavirus
IFN γ	Interferon-gamma
IL-1 β	Interleukin-1 β
EMT	Epithelial–mesenchymal transition
TCGA	The Cancer Genome Atlas
GEO	Gene Expression Omnibus
JCRB	Japanese Collection of Research Bioresources
RT-PCR	Reverse transcription-polymerase chain reaction
GAS	IFN γ activation site
GSEA	Gene Set Enrichment Analysis

Acknowledgements

Not applicable.

Author contributions

HWC, YFL, and CHL designed and coordinated the project. CHL performed the experiments and drafted the manuscript. HLL modified the manuscript and provided valuable advice. YHKL helped perform the experiments and modify the manuscript during revision stage. HHL and HWL helped the designation of experiments and analyzed the data. HWL helped the collection of tissue sample. All authors read and approved the final manuscript.

Funding

This study was supported by the Ministry of Science and Technology, Taiwan (NSTC 112-2314-B-038-087 to Hui-Wen Chiu and MOST 109-2314-B-038-041 to Che-Hsuan Lin), Taipei Medical University (TMU109-AE1-B14 to Che-Hsuan Lin).

Availability of data and materials

Not applicable.

Declarations

Ethics approval and consent to participate

Primary tumors and normal adjacent tissues of OSCC patients were provided by Taipei Medical University Biobank and collected with institutional review board approval (N202204007) and the Declaration of Helsinki.

Consent for publication

Not applicable.

Competing interests

The authors declare that they have no competing interests.

Author details

¹Graduate Institute of Clinical Medicine, College of Medicine, Taipei Medical University, Taipei 11031, Taiwan. ²Department of Medical Research, Shuang Ho Hospital, Taipei Medical University, New Taipei City 23561, Taiwan. ³TMU Research Center of Urology and Kidney, Taipei Medical University, Taipei 11031, Taiwan. ⁴Department of Radiology, School of Medicine, College of Medicine, Taipei Medical University, Taipei 11031, Taiwan. ⁵Department of Radiation Oncology, Taipei Medical University Hospital, Taipei 11031, Taiwan. ⁶Department of Neurology, Taipei Medical University Hospital, Taipei Medical University, Taipei 11031, Taiwan. ⁷Department of Neurology, School of Medicine, College of Medicine, Taipei Medical University, Taipei 11031, Taiwan. ⁸Department of Neurology, Vertigo and Balance Impairment Center, Shuang Ho Hospital, Taipei Medical University, New Taipei City 23561, Taiwan. ⁹Department of Otolaryngology Head and Neck Surgery, Shuang Ho Hospital, Taipei Medical University, New Taipei City 23561, Taiwan. ¹⁰Department of Otolaryngology, Taipei Medical University Hospital, Taipei Medical University, Taipei 11031, Taiwan. ¹¹Department of Obstetrics and Gynaecology, North Shore Private Hospital, Sydney, NSW, Australia. ¹²Department of Gynecology, Ryde Hospital, Northern Sydney Local Health District, Sydney, NSW, Australia. ¹³Northern Clinical School, Faculty of Medicine and Health, The University of Sydney, Sydney, NSW, Australia. ¹⁴Cell Physiology and Molecular Image Research Center, Wan Fang Hospital, Taipei Medical University, Taipei 11696, Taiwan. ¹⁵Department of Otolaryngology, School of Medicine, College of Medicine, Taipei Medical University, 250 Wu-Hsing Street, Taipei 11031, Taiwan.

Received: 18 September 2023 Accepted: 22 December 2023

Published online: 03 January 2024

References

- Mortazavi H, Baharvand M, Mehdipour M. Oral potentially malignant disorders: an overview of more than 20 entities. *J Dent Res Dent Clin Dent Prospects*. 2014;8(1):6–14.
- Dhanuthai K, Rojanawatsirivej S, Thosaporn W, et al. Oral cancer: a multi-center study. *Med Oral Patol Oral Cir Bucal*. 2018;23(1):e23–9.
- Liu C, Wang M, Zhang H, et al. Tumor microenvironment and immunotherapy of oral cancer. *Eur J Med Res*. 2022;27(1):198.
- Zhang Y, Xu X, Cheng H, et al. AIM2 and psoriasis. *Front Immunol*. 2023;14:1085448.
- Wang B, Tian Y, Yin Q. AIM2 inflammasome assembly and signaling. *Adv Exp Med Biol*. 2019;1172:143–55.
- Dihlmann S, Tao S, Echterdiek F, et al. Lack of absent in melanoma 2 (AIM2) expression in tumor cells is closely associated with poor survival in colorectal cancer patients. *Int J Cancer*. 2014;135(10):2387–96.
- Yang Y, Zhang M, Jin C, et al. Absent in melanoma 2 suppresses epithelial–mesenchymal transition via Akt and inflammasome pathways in human colorectal cancer cells. *J Cell Biochem*. 2019;120(10):17744–56.
- Chen J, Wang Z, Yu S. AIM2 regulates viability and apoptosis in human colorectal cancer cells via the PI3K/Akt pathway. *Onco Targets Ther*. 2017;10:811–7.
- Wang D, Zou J, Dai J, et al. Absent in melanoma 2 suppresses gastric cancer cell proliferation and migration via inactivation of AKT signaling pathway. *Sci Rep*. 2021;11(1):8235.
- Zheng J, Liu C, Shi J, et al. AIM2 inhibits the proliferation, invasion and migration, and promotes the apoptosis of osteosarcoma cells by inactivating the PI3K/AKT/mTOR signaling pathway. *Mol Med Rep*. 2022;25(2):53.
- Ma X, Guo P, Qiu Y, et al. Loss of AIM2 expression promotes hepatocarcinoma progression through activation of mTOR-S6K1 pathway. *Oncotarget*. 2016;7(24):36185–97.
- Chen SL, Liu LL, Lu SX, et al. HBx-mediated decrease of AIM2 contributes to hepatocellular carcinoma metastasis. *Mol Oncol*. 2017;11(9):1225–40.
- Zhang M, Jin C, Yang Y, et al. AIM2 promotes non-small-cell lung cancer cell growth through inflammasome-dependent pathway. *J Cell Physiol*. 2019;234(11):20161–73.
- Zheng JQ, Lin CH, Lee HH, et al. AIM2 upregulation promotes metastatic progression and PD-L1 expression in lung adenocarcinoma. *Cancer Sci*. 2023;114(1):306–20.

15. Fukuda K, Okamura K, Riding RL, et al. AIM2 regulates anti-tumor immunity and is a viable therapeutic target for melanoma. *J Exp Med*. 2021;218(9): e20200962.
16. Huang QF, Fang DL, Nong BB, et al. Focal pyroptosis-related genes AIM2 and ZBP1 are prognostic markers for triple-negative breast cancer with brain metastases. *Transl Cancer Res*. 2021;10(11):4845–58.
17. Wang Q, Gao S, Shou Y, et al. AIM2 promotes renal cell carcinoma progression and sunitinib resistance through FOXO3a-ACSL4 axis-regulated ferroptosis. *Int J Biol Sci*. 2023;19(4):1266–83.
18. Jiang L, Ge W, Cui Y, et al. The regulation of long non-coding RNA 00958 (LINC00958) for oral squamous cell carcinoma (OSCC) cells death through absent in melanoma 2 (AIM2) depending on microRNA-4306 and Sirtuin1 (SIRT1) in vitro. *Bioengineered*. 2021;12(1):5085–98.
19. Nakamura Y, Nakahata S, Kondo Y, et al. Overexpression of absent in melanoma 2 in oral squamous cell carcinoma contributes to tumor progression. *Biochem Biophys Res Commun*. 2019;509(1):82–8.
20. Lanczky A, Györfy B. Web-based survival analysis tool tailored for medical research (KMplot): development and implementation. *J Med Internet Res*. 2021;23(7): e27633.
21. Subramanian A, Tamayo P, Mootha VK, et al. Gene set enrichment analysis: a knowledge-based approach for interpreting genome-wide expression profiles. *Proc Natl Acad Sci USA*. 2005;102(43):15545–50.
22. Li T, Fu J, Zeng Z, et al. TIMER2.0 for analysis of tumor-infiltrating immune cells. *Nucleic Acids Res*. 2020;48(W1):W509–14.
23. Chu W, Gao J, Murphy WJ, et al. A candidate interferon-gamma activated site (GAS element) in the HLA-G promoter does not bind nuclear proteins. *Hum Immunol*. 1999;60(11):1113–8.
24. Jin H, Ko YS, Kim HJ. P2Y2R-mediated inflammasome activation is involved in tumor progression in breast cancer cells and in radiotherapy-resistant breast cancer. *Int J Oncol*. 2018;53(5):1953–66.
25. Yu Y, Cao F, Xiong Y, et al. SP1 transcriptionally activates NLRP6 inflammasome and induces immune evasion and radioresistance in glioma cells. *Int Immunopharmacol*. 2021;98: 107858.
26. Tan Y, Wang Z, Xu M, et al. Oral squamous cell carcinomas: state of the field and emerging directions. *Int J Oral Sci*. 2023;15(1):44.
27. Ponomareva L, Liu H, Duan X, et al. AIM2, an IFN-inducible cytosolic DNA sensor, in the development of benign prostate hyperplasia and prostate cancer. *Mol Cancer Res*. 2013;11(10):1193–202.
28. Zhao T, Li Y, Zhang J, et al. PD-L1 expression increased by IFN-gamma via JAK2-STAT1 signaling and predicts a poor survival in colorectal cancer. *Oncol Lett*. 2020;20(2):1127–34.
29. Ahmed KM, Li JJ. NF-kappa B-mediated adaptive resistance to ionizing radiation. *Free Radic Biol Med*. 2008;44(1):1–13.
30. Pordanjani SM, Hosseinimehr SJ. The role of NF-kB inhibitors in cell response to radiation. *Curr Med Chem*. 2016;23(34):3951–63.
31. Tang D, Tao D, Fang Y, et al. TNF-alpha promotes invasion and metastasis via NF-kappa B pathway in oral squamous cell carcinoma. *Med Sci Monit Basic Res*. 2017;23:141–9.
32. Brierly G, Celentano A, Breik O, et al. Tumour necrosis factor alpha (TNF-alpha) and oral squamous cell carcinoma. *Cancers (Basel)*. 2023;15(6):1841.
33. Brassesco MS, Roberto GM, Morales AG, et al. Inhibition of NF-kappa B by dehydroxymethyl epoxyquinomicin suppresses invasion and synergistically potentiates temozolomide and gamma-radiation cytotoxicity in glioblastoma cells. *Chemother Res Pract*. 2013;2013: 593020.
34. Hua X, Ge S, Zhang M, et al. Pathogenic roles of CXCL10 in experimental autoimmune prostatitis by modulating macrophage chemotaxis and cytokine secretion. *Front Immunol*. 2021;12: 706027.
35. Hegde PS, Karanikas V, Evers S. The where, the when, and the how of immune monitoring for cancer immunotherapies in the era of checkpoint inhibition. *Clin Cancer Res*. 2016;22(8):1865–74.
36. Galon J, Bruni D. Approaches to treat immune hot, altered and cold tumours with combination immunotherapies. *Nat Rev Drug Discov*. 2019;18(3):197–218.
37. Reijers ILM, Rao D, Versluis JM, et al. IFN-gamma signature enables selection of neoadjuvant treatment in patients with stage III melanoma. *J Exp Med*. 2023;220(5): e20221952.
38. Guo M, Ye L, Yu T, et al. IL-1beta enhances the antiviral effect of IFN-alpha on HCV replication by negatively modulating ERK2 activation. *ACS Infect Dis*. 2020;6(7):1708–18.
39. Numata Y, Akutsu N, Ishigami K, et al. Synergistic effect of IFN-gamma and IL-1beta on PD-L1 expression in hepatocellular carcinoma. *Biochem Biophys Rep*. 2022;30: 101270.
40. Bemelmans MHA, van Tits LJH, Buurman WA. Tumor necrosis factor: function, release and clearance. *Crit Rev Immunol*. 2017;37(2–6):249–59.
41. Morgado M, Sutton MN, Simmons M, et al. Tumor necrosis factor-alpha and interferon-gamma stimulate MUC16 (CA125) expression in breast, endometrial and ovarian cancers through NFkappaB. *Oncotarget*. 2016;7(12):14871–84.
42. Tsukamoto M, Imai K, Ishimoto T, et al. PD-L1 expression enhancement by infiltrating macrophage-derived tumor necrosis factor-alpha leads to poor pancreatic cancer prognosis. *Cancer Sci*. 2019;110(1):310–20.
43. Kujan O, van Schaijk SB, Farah CS. Immune checkpoint inhibitors in oral cavity squamous cell carcinoma and oral potentially malignant disorders: a systematic review. *Cancers (Basel)*. 2020;12(7):1937.
44. Polverini PJ, D'Silva NJ, Lei YL. Precision therapy of head and neck squamous cell carcinoma. *J Dent Res*. 2018;97(6):614–21.

Publisher's Note

Springer Nature remains neutral with regard to jurisdictional claims in published maps and institutional affiliations.

Ready to submit your research? Choose BMC and benefit from:

- fast, convenient online submission
- thorough peer review by experienced researchers in your field
- rapid publication on acceptance
- support for research data, including large and complex data types
- gold Open Access which fosters wider collaboration and increased citations
- maximum visibility for your research: over 100M website views per year

At BMC, research is always in progress.

Learn more biomedcentral.com/submissions

